A study on the benefits of using variable stiffness feet for humanoid walking on rough terrains

Irene Frizza, Hiroshi Kaminaga, Ko Ayusawa, Philippe Fraisse, Gentiane Venture

A study on the benefits of using variable stiffness feet for humanoid walking on rough terrains

Irene Frizza[1,2], Hiroshi Kaminaga[1], Ko Ayusawa[1], Philippe Fraisse[2], Gentiane Venture[1,3]

***Abstract*— This work aims to study the effects of the variable stiffness of a compliant foot on humanoid locomotion performance. Through dynamical simulations, we demonstrate that the introduction of the variable stiffness feet, changing in conjunction with the ground roughness significantly improves the walking performance on different types of rough terrain of a humanoid robot. We propose a compliant foot model with multiple viscoelastic elements in the sole. We optimize the sole stiffness for different types of uneven terrains: with rocks, tiles, and obstacles of different shapes and dimensions. We implement a variable stiffness method according to the ground roughness during the walking. Furthermore, the timing of ground scanning and optimal stiffness estimation throw the k-nearest neighbors (KNN) algorithm is described. The comparison of the results obtained with completely flat sole, compliant sole with fixed stiffness, and compliant sole with variable stiffness show the superiority of the variable stiffness feet over the two others. Finally, we present some limitations of the flexible robotic foot in the dynamic simulation.**

I. Introduction

Most robotic feet have a flat and rigid structure and are therefore not deformable [1]–[5]. However, maintaining balance on uneven terrain is of paramount importance for robots. To tackle this issue, in recent years, several solutions have been proposed. Some multi-joints feet [6]–[10] structures have been developed. Also, some structures incorporate elastic elements such as springs and dampers [9], [11], [12]. Others contain a rubber layer under the foot sole to adapt it to the ground and absorb impacts [2], [5], [13].

Finding the appropriate viscoelastic properties of such robot feet is an essential process for designing new compliant feet. Finding the optimal values of the viscoelastic properties of the foot given certain rough terrains can guide the design of new robotic feet. However, increasing softness in the foot sole can reduce stability in balancing performance [14]–[16]. Indeed, the risk of falling due to oscillations during the standing phase is greater for structures containing multi-joints and elastic properties. For this reason, the need for an adequate foot compliance model is very important [15].

Introducing soft-behavior elements into dynamic simulation is generally a more difficult simulation problem compared to most robotics simulations which often assume that both the robot and the objects with which it operates are mechanically rigid [17]. Simulators that can also support the contact dynamics between the soft and the rigid elements are necessary. For example, MuJoCo and NVIDIA Isaac support the simulation of deformable objects.

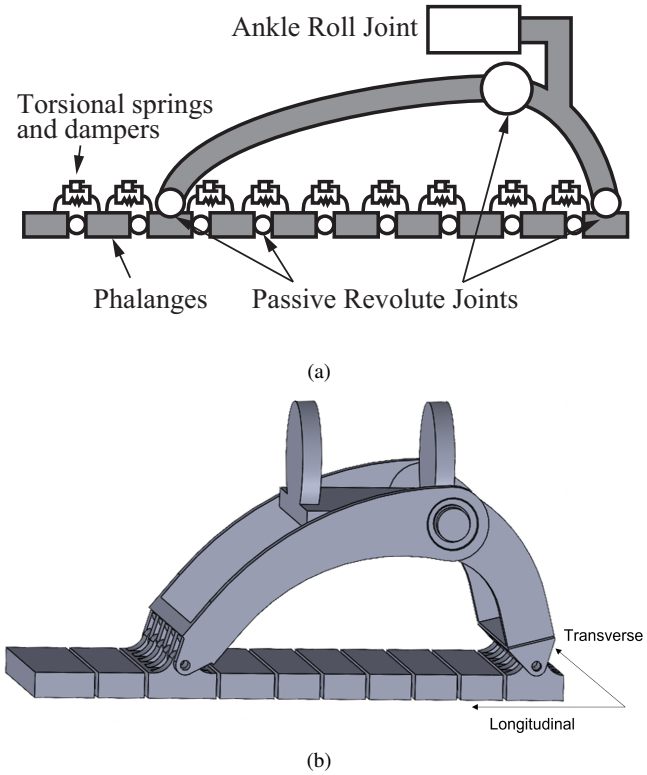

Fig. 1. (a) Simplified model of the compliant foot. The plantar arc is composed of ten blocks representing the ten phalanxes, connected between each other by rotational joints with viscoelastic elements. The plantar arch is connected with the frontal and backward arch through rotational passive joints. (a) Deformable foot model used in dynamic simulation.

Since grounds on which robots operate may vary widely, robotic feet with variable stiffness, i.e. compliance changing according to the terrain, may offer a robust solution. Choi et al. [18] introduced variable compliant humanoid foot design using a leaf spring and rubber balls in series. This promising approach of variable compliance feet is still very rare in the literature for humanoid robots [19]. For now, the studies of variable stiffness structures are almost entirely limited to the field of prostheses. Semiactive prosthetic devices that adjust their stiffness during swing phases are developed to minimize size, mass, and power consumption [20]–[22]. Here, the deformation of the foot allows the foot to overturn during walking, mimicking the response of a biological ankle [22]. In this article, for the first time, we address the problem of a humanoid robot using variable stiffness feet on uneven

[1] CNRS-AIST JRL (Joint Robotics Laboratory), UMI3218/RL, Tsukuba, Ibaraki, Japan.
[2] LIRMM, Université de Montpellier, CNRS Montpellier, France.
[3] The University of Tokyo, Japan.
Corresponding author: irene.frizza@aist.go.jp

terrain in a dynamic simulation of walking. In Sec. II, we present the developed foot model with soft contact, its integration in a simulation environment, and the walking control law. In Sec. (III), we detail our contribution regarding the parameters selected for the simulation environment and sole stiffness optimization. Finally, in Sec. IV, we analyze the method to vary the compliance of the sole according to the ground roughness during the walking and optimal stiffness estimation. In Sec. VI, dynamic simulation experiments of walking are described. Simulation experiments are carried out with the humanoid robot HRP-4J [23].

II. Foot modeling with soft contacts

A. Foot modeling and integration in Mujoco

The ability to perform dynamic simulations quickly and efficiently is necessary to test walking in multiple experimental conditions: environments, terrains, foot parameters. Introducing deformable foot behaviors into a dynamic simulation of the humanoid robot requires a reliable and consistent dynamics simulation environment. Inspired by the robotic foot SoftFoot [6], we developed a simplified CAD model in SolidWorks to evaluate the performance mainly in the forward walking direction (showed in Fig.1(b)).

In order to integrate it into Mujoco, we developed the hierarchical xml model of the simplified foot model. Here, we aim to replicate the three main characteristics of SoftFoot:

1) The deformable plantar fascia: the plantar arch consists of ten cuboid-shaped blocks representing the ten phalanges of the real foot. Each block replicates the same longitudinal and lateral dimensions of the real foot. The blocks are connected with revolute joints and they can rotate along the transverse axis. In order to provide visco-elasticity properties to the plantar arc of the foot, we added torsional springs and damping between the ten blocks of the plantar arc into dynamic environment (Fig.1(a)). The visco-elasticity parameters of the foot arch are decisive to obtain the walk on uneven ground. In fact, as confirmed by the experimental results obtained in [16], a too rigid plantar fascia greatly limits the success of walking on obstacles. Therefore, it is important to properly tune the value of these parameters.
2) The completely passive system: the plantar arch is connected to the ankle by two arches: frontal arch and backward arch. The backward arc is rigidly attached to the ankle platform and it is connected with the front arch through a passive joint, allowing the rotation of the front arc along the pitch axis. The backward arc is connected with the foot sole throw a passive joint. Finally, all the revolute joints connecting the phalanges of the sole are passive, making the foot completely passive (Fig.1(a)).
3) The close kinematic chain: the frontal arch is connected to the sole with a passive joint in order to close the kinematic chain of the foot. Indeed, there is a geometrical constraint between the frontal arch and the third phalanx of the sole. Thanks to this geometrical constraint, the two bodies are anchored to each other and they can rotate around the pitch axis.

B. Soft Contact Models

Contact between phalanges

In the simulation with compliant feet, the contact between two phalanges consists of a virtual spring-damper system, with spring constant $k > 0$ and damper constant $b > 0$. The spring and damper constants are the same for all the phalanges. When the foot is in a flat position, the angles between the phalanges are null and the equilibrium position of the springs is reached (Fig.1(a)). Springs and dampers create passive forces along pitch axis of the foot between the phalanges. As result, the sole is compliant along the walking direction.

Contact between frontal arch and ankle

The frontal arch is free to rotate around the rotational axis of the joint between frontal and backward arc. The contact between the frontal arch and the ankle is modeled, as in the case of the phalanges of the sole, with a spring-damper system. Here, the values of the stiffness and damping constants are fixed to $k = 100\mathrm{Nm/rad}$ and $b = 80\mathrm{Nms/rad}$.

Contact between frontal arc and sole

As explained, we added a constraint between the frontal arch and sole to close the kinematic chain of the foot in the hierarchical model. The dynamic contact between the frontal arch and the foot sole is modeled as follow:

$$a = (1 - d)a_0 - dbv - dkr \tag{1}$$

where a, v and r are respectively the joints acceleration, velocity and position. a_0 is the unforced acceleration and d the impedance. In particular, we defined d position dependent $d(r)$ in a range between $0.9\mathrm{rad/Nms^2}$ and $0.95\mathrm{rad/Nms^2}$. In this way, we have quite hard constraint because values of $d(r)$ close to 0 correspond to soft constraints while values of $d(r)$ close to 1 correspond to hard constraints. Moreover, we have chosen to use not constant value but position dependent value to take the advantage of interpolating property to avoid numerical instability. Thanks to the first term on the right-hand side, the solver interpolate between the unforced acceleration a_0 and the reference acceleration $a_r = -bv - kr$. The stiffness and damping values are defined as follow:

$$b = \frac{2}{d_{max}t}; k = \frac{d(r)}{d_{max}^2 t^2 \zeta} \tag{2}$$

where $d_{max} = 0.95\mathrm{rad/Nms^2}$, t is the time constant and ζ is the damping ratio. We set $t = 2\mathrm{ms}$ and $\zeta = 1$. $\zeta = 1$ corresponds to critical damping. In fact, using smaller values results in under-damped constraints, while using larger values results in excessively damped constraints.

Contact between sole and ground

The dynamic contact between the foot sole and the ground is modeled as in (1). Here, d is set to 0.99 in order to reduce the slip effect during walking. Increasing the constraint impedance can be particularly effective to avoid slip behaviour between the sole and the ground. For this contact equation, $t = 0.1\mathrm{ms}$ and $\zeta = 1$ are set.

TABLE I

PARAMETERS BOUNDS LIMITS USED IN THE BAYESIAN OPTIMIZATION.

Parameter	Lower bound	Upper bound
k	0 Nm/rad	80 Nm/rad
k_P	0.1	5
k_D	0.1	5

TABLE II

OPTIMIZATION OF STABILIZER GAINS AND SOLE STIFFNESS.

Ground Type	Optimal gains		Optimal k
	k_P	k_D	(Nm/rad)
Flat floor	3.4	2.1	Entire Range
Cylinder obst	4.8	1.8	0.2−9.5
Stones	4.0	1.3	2.8−16.1
Small stones	4.3	2.4	2.3−31.6
Stones Bricks	5.0	0.5	25.4−28.9
Pyramidal stones	4.2	1.6	0.9−48.7
Metal iron sheets	3.6	2.7	0.7−19.9
Large floor tiles	3.9	2.6	0.02−0.6
Roof tiles	4.1	2.6	23.9−33.3
Cobble stones	4.0	2.6	18.4−32.8
Floor tiles	3.7	1.1	31.6−46.1

C. Controller in simulation: LIPM walking stabilizer

In the dynamic simulations, we used the dynamic simulator Mujoco, the interface for simulation and robot control systems *mc_rtc* [24] and the controller already established LIPM walking stabilizer [25].

The robot is modelled with a linear inverted pendulum to generate the center of mass (CoM) acceleration for *mc_rtc*. The walking controller [26] used is a position-controller with two main components for the stabilization: the DCM (Divergent Component of Motion) feedback control, which modifies the CoM acceleration based on the DCM estimation and computes the desired contact wrenches to compensate deviation from the walking pattern; and the Whole-body Admittance Control, which allows the robot to realize the desired contact wrench computing commanded velocity and acceleration of the joints. The feedback law expressed in terms of the ZMP is:

$$\begin{aligned} \ddot{p}_c = \ddot{p}_c^d + \omega(k_P \epsilon_{DCM} + \epsilon_{CoM} K_{CoM}) + \\ \omega(k_I \epsilon_{DCM}) + \omega(k_D \dot{\epsilon}_{DCM}) - \omega^2 k_{zmp} Z\dot{M}P^d \end{aligned} \tag{3}$$

where p_c is the CoM position, p_c^d is the desired CoM position, k_P, k_I, k_D are the proportional, derivative and integral constants of the control law, $\omega = \sqrt{g/CoM}$ and ϵ_{DCM} and ϵ_{CoM} are the DCM and CoM errors. In our context, we define $K_I = 0$ because we are using DCM bias estimator. It's purpose is to reduce the average error of DCM to zero. As the integral term of the control law uses the same quantity, we decided to set it to zero.

III. PARAMETERS OPTIMIZATION

A. Parameters selection

After creating the environment with compliant feet for the dynamic simulation, our goal is to select the most appropriate combination of parameters to improve the walking on uneven terrains and obstacles of different shapes and dimensions. In particular, the parameters we analyzed are the proportional and derivative coefficients of the LIPM walking stabilizer (k_P and k_D in (3)) and the stiffness coefficient of the spring-damper system between the phalanges of the foot (k in (2)). The reason why we do not consider the damping constant in the parameter set is that analyzing the passive forces acting between the phalanges of the humanoid foot during walking, the contribution of the damping force is negligible compared to the contribution of the stiffness force. In fact, only a high-frequency noisy contribution is added due to the damper. For this reason, we do not include the damper coefficient (b in 2) in the tuning problem and we fix this term to $2\mathrm{Nms/rad}$. Looking at the simulation, we choose $2\mathrm{Nms/rad}$ because it is a realistic value that empirically mimics the real foot behavior.

B. Bayesian optimization

We used Bayesian optimization to find the best combination of the sole stiffness coefficient and PD gains of the stabilizer of different types of ground. An a posteriori Gaussian distribution is constructed. After each computation, the value of the cost function is calculated. To find an optimal combination of the three parameters, at each optimization step the algorithm is adapted to the samples known from the previous steps. In this way, the next point to be explored is determined. This minimizes the number of steps required to find an optimal combination of parameters [27].The bayesian optimization problem is:

$$\max_{x \in A} J(x) \tag{4}$$

where x is the vector of the variable we are minimizing: $x = \begin{bmatrix} \epsilon_D, & \mu_Z, & \sigma_Z, & \mu_C, & \sigma_C \end{bmatrix}$.

ϵ_D is the number of steps performed without falling. We define:

$$\begin{cases} \epsilon_Z = ZMP_r - ZMP_m \\ \epsilon_C = CoM_r - CoM_m \end{cases} \tag{5}$$

where ZMP_r, CoM_r and ZMP_m and CoM_m are respectively the reference values, the measured values of the Zero Moment Point (ZMP) and of the CoM. μ_Z and σ_Z are respectively the mean value and standard deviation of the ZMP error ϵ_Z, and μ_C and σ_C are respectively the mean value and standard deviation of CoM error ϵ_C. $J(x)$ is the following cost function:

$$J(x) = -\begin{bmatrix} \lambda_D, & \lambda_Z, & \lambda_Z^2, & \lambda_C, & \lambda_C^2 \end{bmatrix} x^\intercal \tag{6}$$

Where the three gains λ_D, λ_Z and λ_C used for the optimization are $[10.0, 3.0, 3.0]$. We have chosen these values of gains to give primary importance to the success or failure of the walking (λ_D) and secondary importance to the quality of the walk in terms of control (λ_Z and λ_C). The range of definition A of the vector x is: $\epsilon_D \in \mathbb{Z}^+, [\mu_Z, \sigma_Z, \mu_C, \sigma_C] \in \mathbb{R}$.

During the Bayesian optimization, the cost is calculated and updated every simulation time step until the robot falls or until the end of the walking path. The optimization selects

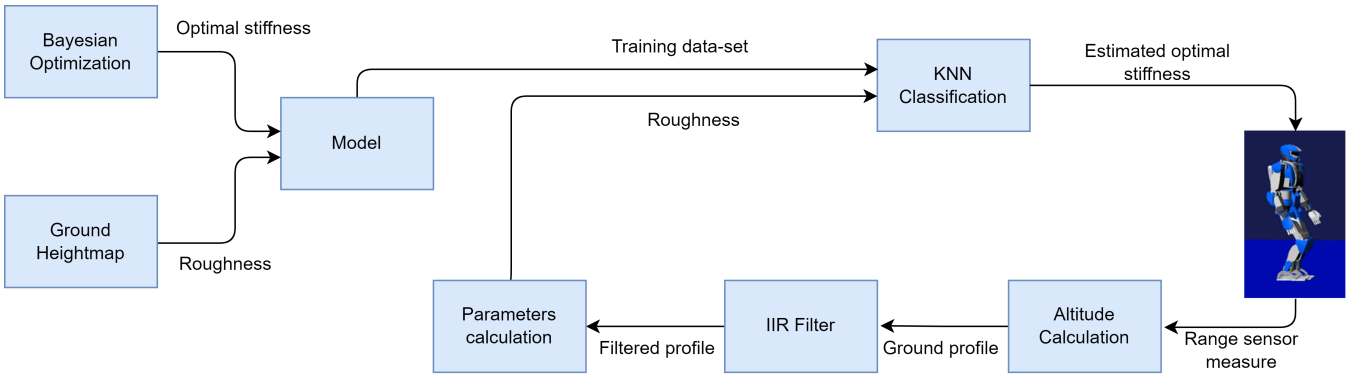

Fig. 2. Proposed method to control the variable stiffness depending on the ground roughness.

the values of the parameters close to the values related to the lowest cost at previous steps. We choose the bounds of the three parameters to include as constraints in the optimization process, taking into account the following considerations. With too large bounds for the torsional springs coefficient k, the number of simulations we need to obtain convergence to optimal stiffness increases significantly, due to a large number of values to test. In addition, the use of too large gains of the stabilizer is not feasible on the real robot. Given the above, we choose stiffness bounds to guarantee a range from very compliant $(0\mathrm{Nm/rad})$ to rigid behavior $(80\mathrm{Nm/rad})$ and gains bounds to guarantee feasibility on the real robot. These values are shown in TableI.

C. Sole stiffness optimization

A total of 4400 simulations are run for the optimization of the sole stiffness and stabilizer gains, on 11 types of uneven grounds with stones, obstacles, and tiles of different sizes and shapes. The task is walking straight forward for a $3m$ distance trajectory (about 22 foot steps). As Table II shows, differently from the stabilizer gains where it is possible to identify a range of work, the optimal range stiffness is noticeably different depending on the type of ground. For example, for walking on large floor tiles the optimal k range is $0.02 \sim 0.6\mathrm{Nm/rad}$, quite far from the optimal range of roof tiles $23.9 \sim 33.3\mathrm{Nm/rad}$. For this reason, it is difficult to identify a single optimal value to designate sole compliance. This result suggests the necessity of using variable stiffness sole design for humanoid robots to walk on different types of uneven grounds.

IV. Variable Stiffness Foot

From the results obtained in this section III, in a complex ground not uniform in type and size of obstacles, the robot will not be able to walk with a unique value of spring coefficient in the feet soles. To account for this, the robotic foot should feature variable stiffness, with compliance changing to be able to walk in all types of terrain. We developed a variable stiffness method shown in Fig.2.
We note through the previous simulations a correspondence between the characteristics of the ground profile and the stiffness necessary to improve the performance. This suggests the study of parameters that define the shape and variation of the terrain.

A. Stiffness variation method depending on ground roughness

To vary the compliance of the sole according to the characteristics of the underlying terrain, the properties of the ground geometry were analyzed. Properties of the surface geometry are generally labeled surface roughness parameters [28]. Table III shows the ground roughness parameters analyzed in this paper and how they are calculated. In the description of the parameters, z_i is the ground altitude values, n is the total number of points considered on the ground and Z_i is the Fourier transform of z_i. Amplitude parameters are the most important parameters to characterize surface topography. They are used to measure the vertical characteristics of the surface deviations. The parameters M, P, and K use the Fourier Analysis to study the surface irregularities, to have a consistent representation in the frequency domain.

To obtain a measure of the roughness of each terrain, the ground altitude values are extracted from heightmaps of different types of terrains. The ground altitude of each

TABLE III
ROUGHNESS PARAMETERS OF THE GROUND PROFILE. [28] [29]

Parameter	Description
S_a	$\frac{1}{n}\sum_{i=1}^{n}\lvert z_i\rvert$
S_q	$\sqrt{\frac{1}{n}\sum_{i=1}^{n} {z_i}^2}$
S_{sk}	$\frac{1}{{S_q}^3}[\sum_{i=1}^{n}\frac{{z_i}^3}{(i+1)}]$
S_{ku}	$\frac{1}{{S_q}^4}[\sum_{i=1}^{n}\frac{{z_i}^4}{(i+1)}]$
S_v	$\lvert min(z_i)\rvert$
S_p	$\lvert max(z_i)\rvert$
S_z	$S_v + S_p$
M	$Var(z(x)) = \sum_0^{N-1}\lvert Z(x)\rvert^2 - \lvert Z(0)\rvert^2$
P	$Var(\dot{z}(x)) = \sum_0^{N-1} {f_0}^2 n^2 \lvert Z(x)\rvert^2$
K	$1 - \frac{\sum_0^{N-1}\lvert Z(x)\rvert^4 - \lvert Z(0)\rvert^4}{(\sum_0^{N-1}\lvert Z(x)\rvert^2 - \lvert Z(0)\rvert^2)^2}$

heightmap frame was obtained by scanning the ground along a $3\mathrm{m}$ long straight trajectory. Consequently, the ground profile of the walking trajectory was reconstructed.

The modeled foot can deform along the walking direction and, therefore, can adapt to the ground irregularities along this direction. Below a ground frequency threshold, the foot will not enter in contact along all ground profiles. For this reason, the ground profile is filtered with a low pass infinite impulse response (IIR) filter with Butterworth design, a cutoff frequency given by the inverse of the foot length, and a sampling rate of $400\mathrm{Hz}$. Subsequently, with the altitude of the filtered ground profile, the roughness parameters were calculated.

B. Estimating optimal stiffness with KNN classification

At this point, we need to understand how to connect the sole stiffness variation with the calculated roughness parameters.

Through the Singular Value Decomposition (SVD) and QR decomposition, we analyzed the incidence of roughness on the sole stiffness. In particular, a matrix with all the roughness coefficients of the different terrains until powers up to the third is considered. In addition, considering the condition number of the matrix, we selected the most influential parameters in the stiffness variation: S_p, P, P^2, S_{ku}^3, P^3, and S_p^3.

We use k-nearest neighbors (KNN) algorithm to classify the data of roughness in order to predict correctly the sole stiffness. In our implementation 10 neighbors are used for each point. In our prediction, the points are weighted by the inverse distance to the new point. The distance metric used is a standard Euclidean distance and the algorithm used to compute the nearest neighbors is KDTree.

For the model training, the data-set is composed of 360 data: 210 are relative to grounds with unique-directional variation along the walking direction, and 150 are relative to grounds with variation in all directions. The first type of ground can provide a consistent result, as the robotic foot can deform only in the walking direction. Heightmaps of these grounds are constructed from a generated random signal of 5 amplitudes between $19.5\mathrm{mm}$ and $38.1\mathrm{mm}$ filtered by a low-pass filter with 7 cut-off frequencies between 0.0001 and $0.1\mathrm{m}^{-1}$. The second type of grounds is more realistic terrains with variation also along the transversal direction. Fig.3 shows the 5 types of grounds used for data-set training of the model: cylinder-shaped obstacles, pyramidal-shaped stones, floor tiles, cobblestones, and ellipsoidal-shaped obstacles. Here, for each of these grounds, we used data relative to 5 different ground amplitudes between $10\mathrm{mm}$ and $40\mathrm{mm}$. For both the two categories, 6 different trajectories are considered for the roughness calculation of each ground. A total of 6,000 simulations were run to construct the training data set (100 for each ground type and each ground amplitude). In the optimization, we fixed the stabilizer gains to $k_P = 3.4$ and $k_D = 2.1$ and we optimize only the sole stiffness parameter. Note that we use stabilizer gains that are optimal for flat feet.

The stiffness values are arbitrarily grouped in 20 clusters of range $4\mathrm{Nm/rad}$. The model predicts the cluster relative to the roughness parameters. We perform k-fold cross-validation with 10 folds. The model has an accuracy of 0.8 with a standard deviation of 0.16. Principal components analysis shows that more than 87% of variance is explained by the first two components.

C. Range sensors and variable stiffness implementation

As explained in IV-A, the roughness of the data-set needed for the training of the KNN model is calculated thanks to the heightmap data of the grounds 2. In order to generalize our method, the goal is to walk on unknown rough terrains, in which the altitude and roughness of the ground are not known a priori. For this reason, a range sensor is placed under the first phalanx of the sole, on the tip of each foot. The position of the sensor on the tip of the foot allows for scanning of the entire area of the ground where the foot will land on the next step. During the walk, the phase in which the robot has one foot on the ground and one foot swinging is called Single Support Phase (SSP). During the simulation, the range sensor of each swing foot scans the ground when in the air in SSP. The altitude of the ground is reconstructed by the knowledge of the sensor pose relative to the fifth phalange and the phalange pose in the global frame. In the first 75% of the SSP, the altitude data are collected 4(c) 4(d). At 75% of SSP, the optimal sole stiffness is calculated through the KNN classification and it is set on the relative foot. During each step of the walking, the ground profile is reconstructed through the range sensor of the foot in the fly and the proper sole stiffness is set 4(e) 4(f). Thinking of a realistic problem, the stiffness value setting could not be instantaneous but the foot design will need time to set the stiffness. For this reason, last 25% of the SSP will be used for the stiffness setting, so that when the foot lands on the ground the stiffness has been adequately set. From the KNN classification, at 75% of the SSP, the optimal cluster is identified. To minimize the error, the mean value between the cluster boundaries is set as the sole stiffness value.

V. Experimental setup

We conducted walking simulations with the same robot and three types of sole: the original flat sole of the humanoid robot, the flexible sole with fixed stiffness set to $5\mathrm{Nm/rad}$, and the flexible sole with variable stiffness changing depending on the ground roughness. Note that the chosen fixed stiffness value was the central value of the optimal range on a wide range of terrains as result of optimization. It is also close to the estimated stiffness in

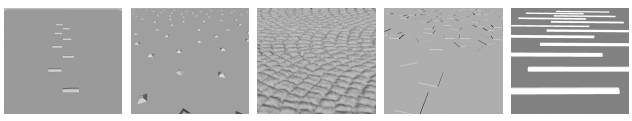

Fig. 3. Types of grounds: Cylinder Obstacles (a), Pyramidal stones (b), Cobble Stones (c), Floor Tiles (d), ellipsoidal-shaped obstacles (e)

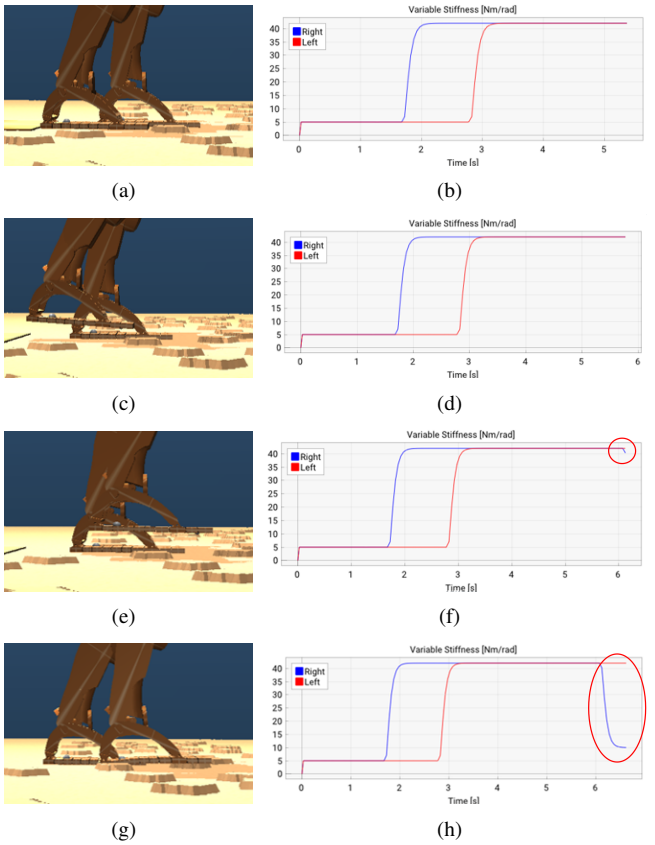

Fig. 4. The sequence of one step with the right foot of the humanoid robot. In (a), both feet are in contact with the ground. The stiffness value of the right foot (blue plot) is $42\mathrm{Nm/rad}$: this value is the result of the previous step scanning (b). Subsequently, in the first 75% of the SSP, the right foot is scanning the ground (c). Here, the altitude data are collecting and the stiffness is still the result of the previous step scanning (d). At 75% of the SSP (e), the stiffness for the right foot is calculated and the blue plot is updating the value to the result of the current step scanning (f). Finally, the right foot is again in contact with the ground (g) and the stiffness value is updated following the result of the scanning (h).

the SoftFoot, already tested on the real robot when walking over obstacles [16]. For these simulations we used several grounds as described below. The test involves walking along a 3m long straight trajectory.

Types of ground

Experiments were performed in two types of ground:

- Unidirectional variation ground. As explained in Sec. IV, these types of terrain allow obtaining consistent results considering the flexibility of the foot along the same direction. For the testing, new ground signals were generated with 4 different amplitudes (20, 25, 30, and 35 mm) and 7 different frequencies (0.0002, 0.0007, 0.002, 0.007, 0.02, 0.07, and 0.2 m^{-1}). The test involves walking the 24 amplitude-frequency combinations of the terrain. The signals that generate these ground profiles are all different from the data that constitute the training data-set for the KNN method.
- Bidirectional variation ground. Fig.4 shows more realistic double-directional variation terrains used to test the

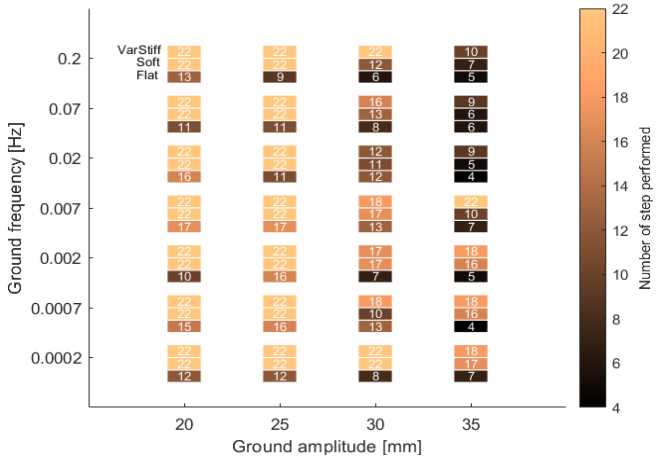

Fig. 5. Comparison of variable stiffness, soft and flat foot performances in unique directional variation ground. The grounds are generated with signals of different amplitudes (horizontal axis) and frequencies (vertical axis). The color of the plot represents the number of steps without falling in a $3\mathrm{m}$ long straight trajectory (about 22 steps). The groups of three squares represent variable stiffness, soft, and flat foot performances respectively on the top, center, and bottom.

walking. Here, the objective is to test the humanoid walking on the more realistic ground with rocks of different shapes and sizes, obstacles, and tiles. Adding the transverse direction of ground variation, the test becomes much more challenging considering that the foot model is deformable only along the longitudinal axis. For these experiments, additional data relating to bidirectional variation grounds are introduced into the training data-set of the model for variable stiffness.

VI. Results and Discussion

Unidirectional variation ground

Fig.5 shows the comparison of the performances with the three types of sole for the combinations of ground profile amplitude (along the horizontal axis) and frequency (along the vertical axis). For each frequency-amplitude combination, the three blocks represent the variable stiffness sole, the soft sole, and the original flat sole of the robot, respectively at the top, middle, and bottom. The color represents the number of steps the robot performed without falling.

As Fig.5 shows, the humanoid with the original flat sole can not complete the path without falling in this combination of rough terrains. The introduction of the new flexible sole and then of the variable stiffness significantly improves performance and the robot can reach the total number of steps for many of the trials.

Bidirectional variation ground

The Table IV shows, in the first column, the types of grounds used to test the walk of the humanoid with the three soles: stones, roof tiles, stones bricks, small stones, and large floor tiles. Similarly to the unidirectional variation ground, the test involves walking along a $3\mathrm{m}$ long straight trajectory. For each type of terrain, 4 different maximum

vertical heights of the terrain are chosen, as column 2 shows. For each of the heights, we report the number of steps carried out without falling with a maximum of 22 steps to cover the $3\mathrm{m}$, for the three types of the sole.
A substantial improvement in the average walking distance/number of steps is obtained due to the introduction of sole flexibility, as the comparison between columns 'Flat' and 'Soft' shows. The robot with the flat sole only walked 140/440. In particular, rigid soles show difficulty in walking since the lower ground amplitudes. Moreover, a further improvement in the number of steps performed is shown in the column 'VarStiff' with the introduction of the variable stiffness sole and the robot can execute all the path in most of the trials. More specifically, we can observe that the introduction of variable stiffness improves the performance, especially in grounds with stones and large floor tiles. Here, the values used with the variable stiffness sole along some parts of the trajectory are high (around $40\mathrm{Nm/rad}$). Indeed, when parts of terrains require stiffness values far from $5\mathrm{Nm/rad}$, a considerable improvement is obtained due to the introduction of the variable stiffness. Conversely, with terrains like roof tiles and small stones, the advantage offered by variable stiffness is less visible. In fact, here, the fixed stiffness value is close to the optimal value.

Limitation

The introduction of the new compliant sole design causes a backward shifting of the center of mass (CoM) of the humanoid. This creates a slight imbalance of the humanoid in the backward direction during the walking. Considering that no modifications have been made to the controller, the robot stabilizer assumes flat feet parallel to the ground. Indeed, the introduction of the rotoidal joint between the foot frontal arch and the ankle allows the pitch rotation of the sole which is not considered in the actual position estimator. However, despite not being taken into account from a control point of view, the introduction of the compliant sole with variable stiffness is already contributing to better success for walking on uneven grounds.

TABLE IV

COMPARISON OF VARIABLE STIFFNESS, SOFT AND FLAT FOOT PERFORMANCES IN DOUBLE DIRECTIONAL VARIATION GROUND.

Ground Type	Max ground amplitude [mm]	Number of steps (max=22)		
		VarStiff	Soft	Flat
Stones 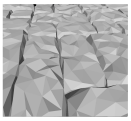	55	20	6	6
	50	22	7	7
	45	22	22	7
	40	22	22	8
Roof tiles 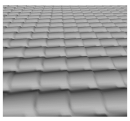	55	8	7	5
	50	22	8	9
	45	22	9	12
	40	22	22	16
Stones bricks 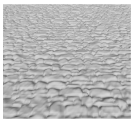	55	8	6	3
	50	22	5	4
	45	22	6	6
	40	22	22	6
Small stones 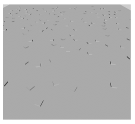	25	9	7	6
	20	13	9	7
	15	22	13	7
	10	22	22	7
Floor tiles 	25	20	8	5
	20	22	12	6
	15	22	19	6
	10	22	22	7

VII. CONCLUSION AND FUTURE WORKS

We presented a compliant foot model with multiple viscoelastic elements in the sole and we optimized the sole stiffness for different types of uneven terrains. We proposed a method to use the surface parameters previously proposed for surface roughness as a vector characterizing the terrains and we used the KNN classifier to detect soil types. We have numerically proven with dynamical simulation tests that foot compliance enhances stability with respect to the rigid sole, and the variable stiffness sole further enhances the stability of humanoid walking in different environments, such as terrains with rocks, tiles, and obstacles of different sizes and shapes. The improvement results with the flexible sole were obtained even using stabilizer gains that are optimal for flat feet. Moreover, even if we introduced flexibility in the sole only along the longitudinal direction, the results have proved effective also for grounds with variation in the transverse direction.

In future works, a new robotic foot for humanoid robots will be designed. A compliant sole with the variable stiffness method connected to the ground roughness will be introduced in a physical experiment. The problem of changing the stiffness on-line during the walking will be faced introducing pneumatic actuation to the sole. Last, we will study how to improve the robot stabilization adapting the robot controller to uneven ground and flexible sole in future work.

REFERENCES

[1] H.-j. Kang, K. Hashimoto, H. Kondo, K. Hattori, K. Nishikawa, Y. Hama, H.-o. Lim, A. Takanishi, K. Suga, and K. Kato, "Realization of biped walking on uneven terrain by new foot mechanism capable of detecting ground surface," in *2010 IEEE International Conference on Robotics and Automation*. IEEE, 2010, pp. 5167–5172.

[2] J. Li, Q. Huang, W. Zhang, Z. Yu, and K. Li, "Flexible foot design for a humanoid robot," in *2008 IEEE International Conference on Automation and Logistics*. IEEE, 2008, pp. 1414–1419.

[3] J. Yamaguchi, A. Takanishi, and I. Kato, "Experimental development of a foot mechanism with shock absorbing material for acquisition of landing surface position information and stabilization of dynamic biped walking," in *Proceedings of 1995 IEEE International Conference on Robotics and Automation*, vol. 3. IEEE, 1995, pp. 2892–2899.

[4] I.-W. Park, J.-Y. Kim, J. Lee, and J.-H. Oh, "Mechanical design of humanoid robot platform khr-3 (kaist humanoid robot 3: Hubo)," in *5th IEEE-RAS International Conference on Humanoid Robots, 2005.* IEEE, 2005, pp. 321–326.

[5] K. Hirai, M. Hirose, Y. Haikawa, and T. Takenaka, "The development of honda humanoid robot," in *Proceedings. 1998 IEEE international conference on robotics and automation (Cat. No. 98CH36146)*, vol. 2. IEEE, 1998, pp. 1321–1326.

[6] C. Piazza, C. Della Santina, G. M. Gasparri, M. G. Catalano, G. Grioli, M. Garabini, and A. Bicchi, "Toward an adaptive foot for natural walking," in *IEEE-RAS 16th Int. Conf. on Humanoid Robots*, 2016, pp. 1204–1210.

[7] J. Yoon, H. Nandha, D. Lee, and G.-s. Kim, "A novel 4-dof robotic foot mechanism with multi-platforms for humanoid robot (sice-iccas 2006)," in *SICE-ICASE Int. Joint Conf.*, 2006, pp. 3500–3504.

[8] S. Yalamanchili, R. Abboud, and W. Wang, "A model to calculate the joint movements and forces in the foot," in *9th Int. Conf. on Electronic Measurement & Instruments*, 2009, pp. 4–532.

[9] J.-T. Seo and B.-J. Yi, "Modeling and analysis of a biomimetic foot mechanism," in *2009 IEEE/RSJ International Conference on Intelligent Robots and Systems*. IEEE, 2009, pp. 1472–1477.

[10] K. Narioka, T. Homma, and K. Hosoda, "Humanlike ankle-foot complex for a biped robot," in *2012 12th IEEE-RAS International Conference on Humanoid Robots (Humanoids 2012)*. IEEE, 2012, pp. 15–20.

[11] K. Hashimoto, Y. Takezaki, K. Hattori, H. Kondo, T. Takashima, H.-o. Lim, and A. Takanishi, "A study of function of foot's medial longitudinal arch using biped humanoid robot," in *2010 IEEE/RSJ International Conference on Intelligent Robots and Systems*. IEEE, 2010, pp. 2206–2211.

[12] D. Kuehn, F. Beinersdorf, F. Bernhard, K. Fondahl, M. Schilling, M. Simnofske, T. Stark, and F. Kirchner, "Active spine and feet with increased sensing capabilities for walking robots," in *International Symposium on Artificial Intelligence, Robotics and Automation in Space (iSAIRAS-12)*, 2012, pp. 4–6.

[13] S. Davis and D. G. Caldwell, "The design of an anthropomorphic dexterous humanoid foot," in *IEEE/RSJ Int. Conf. on Intelligent Robots and Systems*, 2010, pp. 2200–2205.

[14] A. David, J.-R. Chardonnet, A. Kheddar, K. Kaneko, and K. Yokoi, "Study of an external passive shock-absorbing mechanism for walking robots," in *Humanoids 2008-8th IEEE-RAS International Conference on Humanoid Robots*. IEEE, 2008, pp. 435–440.

[15] H. Minakata, "A study of flexible shoe system for biped robot," in *The 8th IEEE International Workshop on Advanced Motion Control, 2004. AMC'04.* IEEE, 2004, pp. 387–392.

[16] M. G. Catalano, I. Frizza, C. Morandi, G. Grioli, K. Ayusawa, T. Ito, and G. Venture, "Hrp-4 walks on soft feet," *IEEE Robotics and Automation Letters*, 2020.

[17] J. Collins, S. Chand, A. Vanderkop, and D. Howard, "A review of physics simulators for robotic applications," *IEEE Access*, 2021.

[18] W. Choi, G. A. Medrano-Cerda, D. G. Caldwell, and N. G. Tsagarakis, "Design of a variable compliant humanoid foot with a new toe mechanism," in *2016 IEEE International Conference on Robotics and Automation (ICRA)*. IEEE, 2016, pp. 642–647.

[19] I. Frizza, K. Ayusawa, A. Cherubini, H. Kaminaga, P. Fraisse, and G. Venture, "Humanoids' feet: State-of-the-art & future directions," *International Journal of Humanoid Robotics*, vol. 19, no. 01, p. 2250001, 2022.

[20] C. Lecomte, A. L. Ármannsdóttir, F. Starker, H. Tryggvason, K. Briem, and S. Brynjolfsson, "Variable stiffness foot design and validation," *Journal of Biomechanics*, vol. 122, p. 110440, 2021.

[21] E. M. Glanzer and P. G. Adamczyk, "Design and validation of a semi-active variable stiffness foot prosthesis," *IEEE Transactions on Neural Systems and Rehabilitation Engineering*, vol. 26, no. 12, pp. 2351–2359, 2018.

[22] H. Tryggvason, F. Starker, C. Lecomte, and F. Jonsdottir, "Use of dynamic fea for design modification and energy analysis of a variable stiffness prosthetic foot," *Applied Sciences*, vol. 10, no. 2, p. 650, 2020.

[23] K. Kaneko, F. Kanehiro, M. Morisawa, K. Akachi, G. Miyamori, A. Hayashi, and N. Kanehira, "Humanoid robot hrp-4-humanoid robotics platform with lightweight and slim body," in *IEEE/RSJ Int. Conf. on Intelligent Robots and Systems*, 2011, pp. 4400–4407.

[24] "mcrtc website," https://jrl-umi3218.github.io/mc_rtc/, accessed: 2021-05-30.

[25] S. Caron, A. Kheddar, and O. Tempier, "Stair climbing stabilization of the hrp-4 humanoid robot using whole-body admittance control," in *Int. Conf. on Robotics and Automation*, 2019, pp. 277–283.

[26] "Lipm walking stabilizer," https://scaron.info/doc/lipm_walking_controller/index.html.

[27] "Bayesian optimization," https://github.com/fmfn/BayesianOptimization.

[28] E. Gadelmawla, M. M. Koura, T. M. Maksoud, I. M. Elewa, and H. Soliman, "Roughness parameters," *Journal of materials processing Technology*, vol. 123, no. 1, pp. 133–145, 2002.

[29] R. Hoffman and E. Krotkov, "Terrain roughness measurement from elevation maps," in *Mobile Robots IV*, vol. 1195. International Society for Optics and Photonics, 1990, pp. 104–114.